SDC

HIGH-RESOLUTION MULTIMODAL IMAGING AFTER IDIOPATHIC EPIRETINAL MEMBRANE SURGERY

MARCO LOMBARDO, MD, PhD,* FABIO SCARINCI, MD,* DANIELA GIANNINI, ME,*†
MARCO PILERI, MD,‡ GUIDO RIPANDELLI, MD,* MARIO STIRPE, MD,*
GIUSEPPE LOMBARDO, ME, PhD,§¶ SEBASTIANO SERRAO, MD, PhD*

Purpose: To investigate the changes of the vitreomacular interface during a 1-year follow-up after idiopathic epiretinal membrane (iERM) surgery.

Methods: Six patients affected by fovea-attached iERM were recruited in this pilot study. Pars plana vitrectomy associated with epiretinal membrane peeling was performed uneventfully in all cases. In four cases, the inner limiting membrane was removed using Brilliant blue G. En face high-resolution adaptive optics and cross-sectional spectral domain optical coherence tomography retinal imaging were performed before and at 1, 3, 6, and 12 months after surgery. The microstructures of vitreomacular interface in high-resolution adaptive optics images were correlated to the cross-sectional spectral domain optical coherence tomography data.

Results: Preoperatively, adaptive optics images showed multiple abnormalities of the vitreomacular interface, such as macrofolds, microfolds, and hyperreflective microstructures. We identified two subtypes of iERM according to the distribution of microfolds over the foveal area, which included the radial-type and the grid-type iERM. After surgery, the morphology of the vitreomacular interface changed compared with the preoperative state. The number of both macrofolds and microfolds was reduced in all cases. The hyperreflective structures were still resolvable in all cases, however presenting different shape and morphology than preoperatively. In addition, they showed marked differences between eyes that had internal limiting membrane removal and eyes that did not.

Conclusion: Adaptive optics imaging gives new insight into the changes of vitreomacular interface after iERM surgery. Enhanced multimodal imaging of the vitreomacular interface and retinal structures can be valuable to monitor treatment outcome of iERM.

RETINA 0:1–10, 2015

Idiopathic epiretinal membrane (iERM) is the most common vitreomacular interface pathology in elderly population. It occurs in 7% of the general population, and its prevalence increases at 11% over 70 years.[1] Treatment options consist of watchful waiting or vitrectomy surgery relative to loss of visual acuity and disorganization of the retina. The recurrence rate within 1 year after surgery is 5% to 10% and reoperation is needed in ~3% of cases.[1,2] The recurrence rate requiring operation has been shown to decrease after internal limiting membrane (ILM) removal.[1,3]

Enhanced visualization of vitreomacular interface and retinal architecture may be valuable for monitoring, surgical planning, and evaluation of surgical outcomes of iERM. The ability to visualize the retina at high resolution may contribute to a better understanding of iERM pathophysiology and may be an aid for surgical decisions. Spectral domain optical coherence tomography (SD-OCT) has greatly improved the visualization of the vitreomacular interface and has become a key tool for the diagnosis and follow-up of patients with iERM.[4–6] High-resolution imaging of retinal cross sections is a well-established method to track progression of epiretinal membrane and monitor treatment outcome.[7–9] In addition, en face three-dimensional reconstruction of SD-OCT images has been shown to provide additional information about the changes of the retinal layers induced by surgery.[10] Overall, three-dimensional en face reconstruction has disclosed a global overview of the abnormalities of

the inner retina and retinal surface with high quality that would not be obtained from cross-sectional scans alone.

Adaptive optics ophthalmoscopy is a novel imaging tool that provides high-resolution images of the retinal microstructures and has been already shown to be valuable to investigate eyes with iERM, providing information either on the photoreceptor layer[11,12] or the vitreomacular interface.[13] In this work, we aimed to evaluate the vitreomacular interface using adaptive optics retinal imaging over 1 year after vitrectomy for iERM. The microstructures of vitreomacular interface in high-resolution adaptive optics images were morphologically correlated to cross-sectional SD-OCT data.

Materials and Methods

All research procedures described in this work adhered to the tenets of the Declaration of Helsinki. The study protocol was approved by the local Ethical Committee (Azienda Sanitaria Locale Roma A), and all subjects recruited gave written informed consent after a full explanation of the procedure.

The inclusion criteria were 1) diagnosis of idiopathic, fovea-attached type, epiretinal membrane according to the SD-OCT classification by Hwang et al[6] (either Group 1A, 1B, or 1C), 2) metamorphopsia tested using the Amsler grid chart, 3) 1.0 logMAR best-corrected visual acuity or better, and 4) 1-mm central retinal thickness (CRT) >300 μm. The exclusion criteria were 1) secondary epiretinal membrane, 2) pseudohole type epiretinal membrane,[6] 3) corneal opacity, 4) astigmatism higher than 3 diopters, 5) previous retinal or glaucoma surgery, and 6) participants already recruited in previous study.[13]

Surgical Procedure

The surgery was performed by two skilled vitreoretinal surgeons (G.R. and M.P.). The procedure was

From the *Fondazione G.B. Bietti IRCCS, Rome, Italy; †Department of Statistical Sciences, University of Rome "La Sapienza", Rome, Italy; ‡Azienda Ospedaliera San Giovanni Addolorata, Rome, Italy; §Consiglio Nazionale delle Ricerche, Istituto di Processi Chimico-Fisici (CNR-IPCF), Messina, Italy; and ¶Vision Engineering Italy srl, Rome, Italy.

Reprint requests: Marco Lombardo, MD, PhD, Fondazione G.B. Bietti IRCCS, Via Livenza 3, 00198 Rome, Italy; e-mail: mlombardo@visioeng.it

based on a standard 3-port pars plana vitrectomy using 23-gauge instruments that included removal of posterior hyaloids and epiretinal membrane peeling with intraocular forceps. After removing the iERM, for patients who underwent ILM peeling, Brilliant Blue G (Geuder, Heidelberg, Germany) was used to stain the inner limiting membrane; in all these cases, a rhexis of 3 disk diameters centered on the foveola was performed using end-gripping forceps. In case of visually significant cataract, the lens was removed and an intraocular lens was implanted during the surgery.

Ophthalmic Testing

Preoperatively and 1, 3, 6, and 12 months after surgery, each patient received a complete eye examination, including best-corrected visual acuity with ETDRS score (expressed as logMAR and Snellen lines), indirect ophthalmoscopy, noncontact ocular biometry using the IOL Master (Carl Zeiss Meditec AG, Hennigsdorf, Germany), retinal imaging using a Spectralis scanning laser ophthalmoscopy (SLO)/ SD-OCT (Heidelberg Engineering GmbH, Heidelberg, Germany), and an adaptive optics retinal camera (*rtx1*; Imagine Eyes, Orsay, France). Central 10° microperimetry (MP1, Nidek Co Ltd, Gamagori, Japan) was performed using a 4-2 threshold strategy with a Goldmann III stimulus size and 37 stimulus locations. The duration of the stimulus was 200 milliseconds, and the fixation target was varied in size according to the patient's best-corrected visual acuity. Numeric thresholds in decibels were exported for statistical analysis.

The SD-OCT images were acquired using the "follow-up scan protocol" by Spectralis that automatically aligns the scans across follow-up examinations during acquisition. For each eye, the preoperative scans were used as reference. The SD-OCT images were acquired in each eye using a volume scan 15° × 10° in the high-resolution modality (numbers of B-scans: 13; distance between each scan: 240 μm; real-time averaging algorithm: 100 frames). The Spectralis software automatically provided 2 contour lines that were positioned at the ILM and the inner edge of the retinal pigment epithelium (interdigitation zone) to measure the 1-mm CRT values. These values included the maximum CRT, minimum CRT, and mean CRT. In addition, the proprietary software was used to segment the 1-mm central inner retinal thickness and the 1-mm central outer retinal thickness. The inner retinal thickness was defined as the distance between the ILM and the outer edge of the outer plexiform layer; the outer retinal thickness was defined as the distance between the outer edge of outer plexiform layer and the interdigitation zone.

A flood-illumination adaptive optics retinal camera was used to acquire images of the vitreomacular interface.[14] Adaptive optics imaging sessions were conducted after dilating the pupils with 1 drop of 1% tropicamide. The plane of focus was adjusted to capture images of the vitreomacular interface using the deformable mirror through the *rtx1* software interface. Digital videos were recorded on several locations covering 8° × 4° around the fovea. For each location, a video of 40 frames (4° field size) was captured by the retinal camera.

A proprietary program provided by the manufacturer was used to correct for distortions within frames of the raw image sequence and to register and frame-average to produce a final image with enhanced signal-to-noise ratio. The final adaptive optics images were automatically stitched together to create a larger montage image of the vitreomacular interface using i2k Retina Pro (DualAlign LLC, New York, NY). The montages were used for registration with images of other imaging modalities by matching the shape of the vessels.

The nonlinear formula of Drasdo and Fowler and the Gullstrand schematic model eye parameterized by the biometry measurements were used to convert each final image from degrees of visual angle to micrometers on the retina.[15,16] Image analysis of the vitreomacular surface was performed using Image J (version 1.45a; NIH, Bethesda, MD; http://imagej.nih.gov/ij).

Statistics

Statistical analysis was performed using the SPSS software (version 17.0; SPSS Inc, Chicago, IL). Two-way analysis of variance for repeated measures was used to compare preoperative and postoperative data and the changes among study cases. Differences with a P of 0.05 or less were considered statistically significant.

Results

Six patients (5 males and 1 female; 60.3 ± 10.5 years) with fovea-attached iERM documented using SD-OCT were recruited in this prospective pilot study (Table 1). Pars plana vitrectomy–associated epiretinal membrane peeling was performed uneventfully in all cases; 4 eyes (Cases 1, 4, 5, and 6) had ILM peeling. Case 1 had simultaneous phacoemulsification and intraocular lens implantation at the time of epiretinal membrane peeling. All patients completed the follow-up protocol, except for Case 6, which was unavailable at 1 year. No limitation for high-resolution adaptive optics imaging of the vitreomacular interface was recorded in eyes with intraocular lens.

Table 1. Preoperative Characteristics of Study Cases

Study Case	Gender	Age, years	Eye	Lens	Surgeon	SD-OCT iERM Subgroup	Adaptive Optics iERM Subgroup	ILM Removal	Axial Length, mm	CRT Max, μm	CRT Min, μm	CRT Mean, μm	IRT, μm	ORT, μm
1	M	64	OS	Intraocular lens	M.P.	1B	Grid	Yes	23.79	568	523	546	342 (63%)	204 (37%)
2	M	48	OD	Intraocular lens	G.R.	1B	Radial	No	23.78	901	489	634	438 (69%)	196 (31%)
3	M	60	OD	Clear lens	G.R.	1B	Grid	No	24.92	725	651	695	446 (64%)	249 (36%)
4	M	73	OD	Intraocular lens	M.P.	1C	Radial	Yes	24.39	449	365	415	220 (53%)	195 (47%)
5	M	48	OS	Clear lens	M.P.	1B	Radial	Yes	25.67	647	552	573	365 (64%)	208 (36%)
6	F	69	OD	Clear lens	M.P.	1A	Radial	Yes	21.23	496	343	403	208 (51%)	195 (49%)
Mean									23.96	631	487	544	336 (62%)	208 (38%)
SD									1.52	165	116	117	103	21

In parenthesis, IRT and ORT values are represented as percentage to the mean CRT. IRT, inner retinal thickness; OD, right eye; ORT, outer retinal thickness; OS, left eye.

Preoperatively, adaptive optics images showed multiple abnormalities of the vitreomacular interface, which included microfolds, macrofolds, and hyperreflective microstructures. The microfolds were defined as folds of the vitreomacular interface with 5 μm to 10 μm width and could not be resolved by SLO or SD-OCT imaging modalities. We identified 2 subtypes of iERM according to the pattern of microfolds over the fovea, such as the radial-type and the grid-type iERM (Figure 1). In radial-type iERM, the microfolds were converging radially toward the fovea, over which they formed plicae or dumps of the vitreomacular interface; in the grid-type iERM, the microfolds were converging toward the fovea, over which they formed grating wrinkles. The epiretinal membrane folds wider than 15 μm were defined as macrofolds and were clearly resolved by SLO. Several hyperreflective structures, relative to their surroundings, were identified in the vitreomacular interface. These microstructures appeared as spots or, more frequently, as irregular lines shorter than 10 μm that were running perpendicular to macrofolds. In cross-sectional SD-OCT images, the hyperreflective structures were associated with different findings of the inner retinal layers (Figure 1).

Preoperatively, the mean CRT ranged between 403 μm and 695 μm; Group 1B iERMs had the thickest inner retinal thickness and Group 1A iERM had the thickest outer retinal thickness relative to the mean CRT (Table 1). The preoperative best-corrected visual acuity ranged between 1.1 and 0.2 logMAR (20/250 and 20/32 Snellen lines, respectively) and the central 10° sensitivity between 15.6 dB and 18.2 dB (see **Table, Supplemental Digital Content 1**, http://links.lww.com/IAE/A350).

At 1 month postoperatively, the morphology of the vitreomacular interface changed relative to the preoperative state. The number of both macrofolds and microfolds was reduced in all cases. The hyperreflective structures were seen in all cases; they however presented different shape and distribution than preoperatively. Over the foveal area, they were mostly clustered showing a ring-shaped morphology; outside the fovea, they were mainly distributed along the nerve

Fig. 1. High-resolution en face adaptive optics and cross-sectional SD-OCT imaging of iERM in three study cases. Scale bars represent 200 μm. **A.** Case 5: the vitreomacular interface shows a number of radial folds converging toward the fovea, where they form a y-shaped fold. The hyperreflective structures are spread nasally from the fovea and perpendicular to the macrofolds; these features were associated with disruption of the retinal nerve fiber layer caused by traction of epiretinal membrane (arrow). The retinal vessels were resolved as faint elements below the wrinkled vitreomacular interface. This case was identified as radial-type iERM. **B.** Case 1: the vitreomacular interface shows several folds forming a gridlike structure across the central retina. The vitreomacular interface shows a bumpy appearance. The hyperreflective microstructures are spread all over the vitreomacular interface and were associated with the presence of fibrous tissue under the epiretinal membrane (arrow). The retinal vessels are not resolved clearly. This case was identified as grid-type iERM. **C.** Case 3: the vitreomacular interface shows a moderate number of folds converging toward the fovea, where they cross each other forming microwrinkles. The hyperreflective microstructures are spread randomly over these features and are associated with high hyperreflectivity of the retinal nerve fiber layer and ganglion cell layer at corresponding location (arrow). The retinal vessels can be well visualized. This case was identified as grid-type iERM.
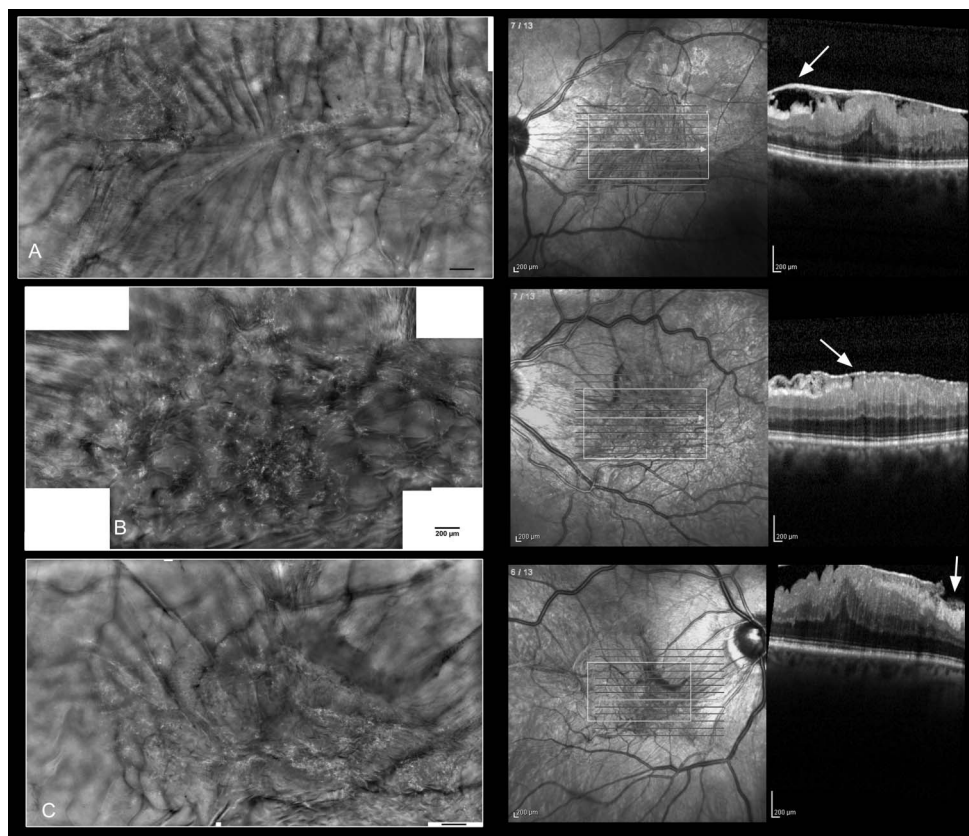
fiber bundles' septa (Figure 2). The latter distribution pattern was only found in eyes that had ILM removal.

At 3 months and 6 months, the macrofolds disappeared in all cases, except for Cases 2 and 3 that had no ILM removal. In both cases, we were able to resolve radial folds temporal and inferior from the fovea, which were stable at 12 months postoperatively. The hyperreflective structures were still numerous in 3 cases (Cases 1, 4, and 6), all of which had ILM removal. In Case 5, several microcysts (30.2 ± 9.3 μm diameter; range, 13–46 μm) were resolved over the vitreomacular interface inferior and temporal from the fovea at 6 months. These microstructures were still resolvable at 12 months and were associated with dimples of the retinal nerve fiber layer and the presence of small fluid abnormalities in the corresponding inner retinal layers in SD-OCT images (Figure 3). The morphology of vitreomacular interface was stable between 6 months and 12 months of follow-up in all cases (Figure 4).

At 1 month, the mean CRT decreased by 118 μm ($P < 0.05$), the mean CRT thinning was >150 μm in all cases, except for Case 4 (+31 μm; $P < 0.001$). At 6 months, the mean CRT was significantly thinner than preoperatively (−152 μm; $P < 0.05$); it remained stable at 1 year postoperatively (−156 μm). At the end of follow-up, the mean CRT and inner retinal thickness decreased more in Cases 2 and 3, which had no ILM removal, than in other cases ($P < 0.001$; Table 2). Overall, the outer retinal thickness was relatively unchanged after surgery ($P > 0.05$), with no or minimal thinning, except for Cases 4 and 6 (+19 and +17 μm, respectively; $P < 0.001$) that showed mild thickening during follow-up.

The visual outcome, the refractive and microperimetry data collected during follow-up were uploaded as **Supplemental Digital Content 2** (see **Table**, http://links.lww.com/IAE/A349).

Discussion

In recent years, high-resolution SD-OCT has greatly improved the visualization of the vitreomacular interface and has become a key tool for the diagnosis and follow-up of patients with alterations of the vitreomacular interface. Software improvement recently permitted en face three-dimensional reconstruction and visualization of the intraretinal structure in the same place as the retinal surface. In cases of epiretinal
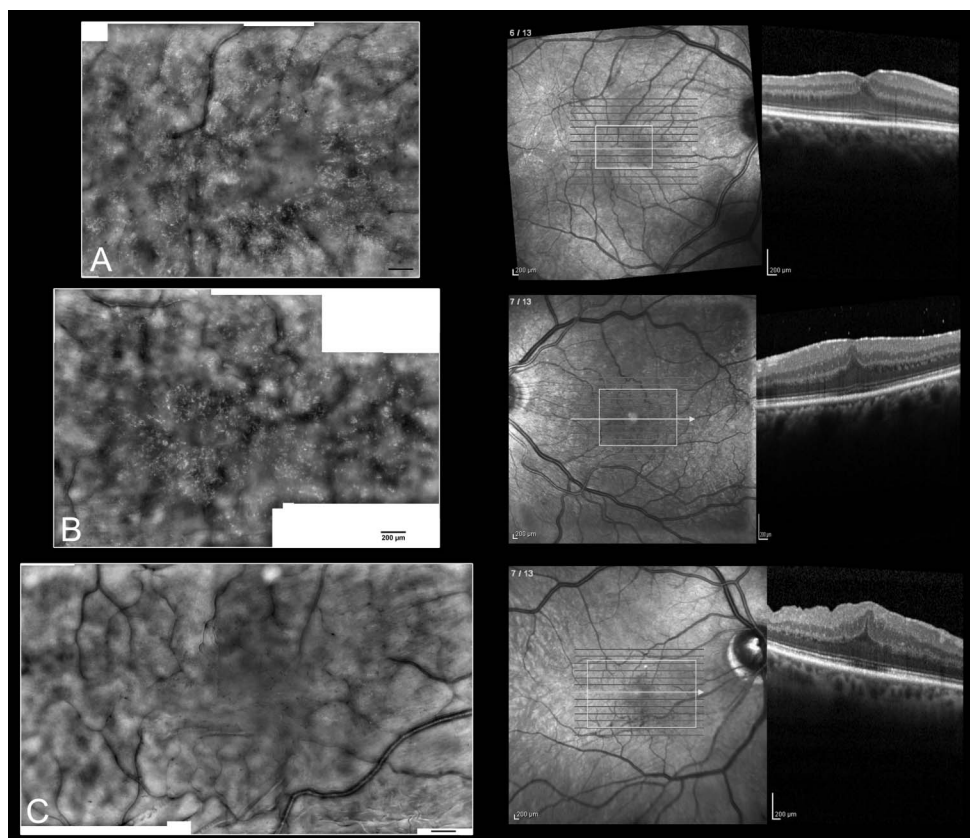
Fig. 2. En face adaptive optics and cross-sectional SD-OCT images of the vitreomacular interface 1 month postoperatively. Scale bars represent 200 μm. The hyperreflective microstructures were still numerous after ILM removal; they greatly decreased in cases that had no ILM removal. In all cases, these features showed different shape and distribution relative to their preoperative morphology. **A.** In Case 6 (radial-type iERM, ILM removed), the hyperreflective microstructures were mainly distributed along the Müller septa, without showing any correlation with abnormal features of SD-OCT retinal images. **B.** In Case 1 (grid-type iERM, ILM removed), they had ring-shaped structure and were spread over the fovea; there were no specific abnormalities of the inner retinal layers in SD-OCT images. **C.** In Case 3 (grid-type iERM, ILM not removed), the vitreomacular interface shows faint and sporadic hyperreflective dots, while still presenting macrofolds and microfolds inferior to the fovea. The retinal nerve fiber bundles could be well appreciated superior to the fovea. The SD-OCT images showed distorted profile of the vitreomacular interface and retinal nerve fiber layer.

Fig. 3. En face adaptive optics and cross-sectional SD-OCT imaging of the retina in Case 5 (radial-type iERM, ILM removed) at 12 months after surgery. Scale bar represents 200 μm. In the adaptive optics retinal montage, the microcysts are shown inferior and temporal from the fovea (arrows). These structures correlated with dimples of the retinal surface and retinal nerve fiber layer in SD-OCT images (arrows) passing through the fovea (top) and inferior (middle and bottom) from the fovea. A small blister of fluid was found in the inner retinal layers below the dimples of the retinal surface (encircled). There were still some dots and ring-shaped hyperreflective microstructures over the fovea.
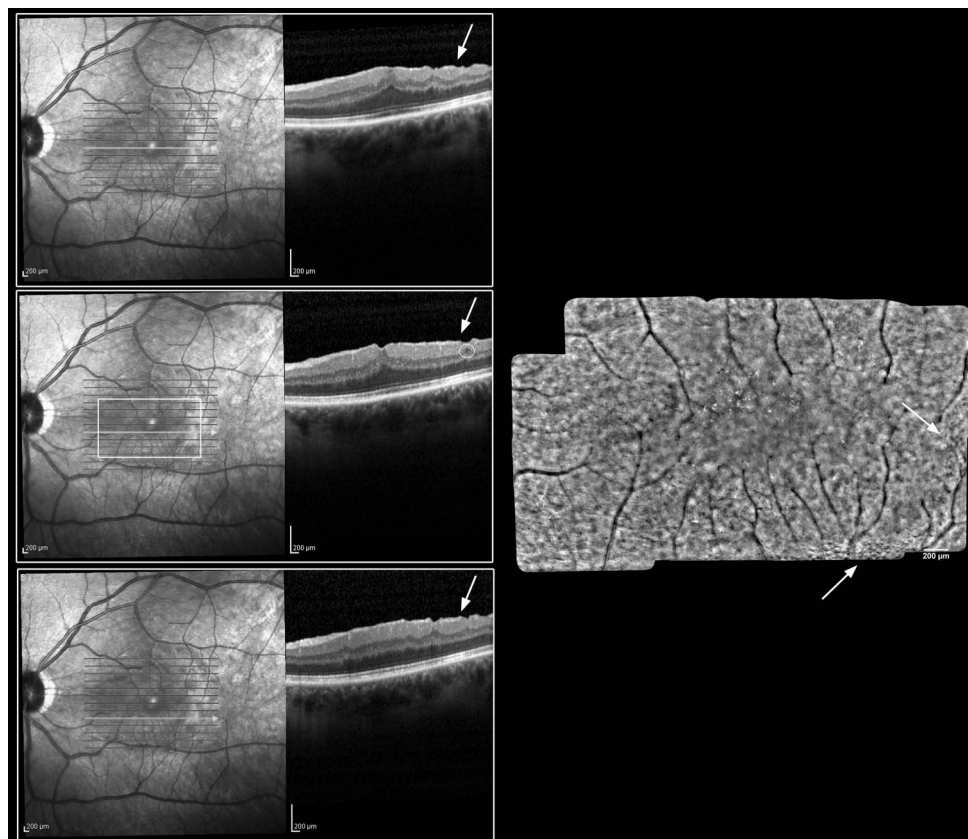
membranes, retinal wrinkling can be seen in the en face image, and the wrinkling of the vitreomacular interface and thickening of the retinal layers in the correspondent cross-sectional SD-OCT image can be observed and easily correlated.

The combination of high-quality SD-OCT and adaptive optics retinal imaging may offer several additional advantages, including an accurate correlation of tomographic with topographic architecture of the inner and outer retina, which may open new insights in the ultrastructural changes induced by surgery.[11,13] In addition, the unprecedented ability to visualize the vitreomacular interface may contribute to a better understanding of iERM and can be an aid for surgical decisions and for assisting to evaluate the outcome of surgery.[13]

In this pilot study, the vitreomacular interface was evaluated using en face adaptive optics retinal imaging during 1-year follow-up after 23-gauge pars plana vitrectomy for iERM. The ultrastructure of the vitreomacular interface was correlated to pathologic changes of the retina through visualization of cross-sectional SD-OCT images. Previous studies have classified iERM based on their appearance on cross-sectional OCT images and have suggested that epiretinal membranes may exert vertical and tangential traction on the retina, leading to distortion of retinal

layers and loss of normal fovea contour.[6] We focused our study to analyze the structures of the vitreomacular interface in fovea-attached type iERM over 1-year follow-up. Preoperatively, adaptive optics imaging revealed several features of the iERM, such as macrofolds, microfolds, and hyperreflective structures. The macrofolds correlated with retinal wrinkles resolved by SLO and SD-OCT imaging, whereas the microfolds could not be detected by conventional instrumentation. The microfolds and macrofolds consist of wrinkles of the vitreomacular interface owing to abnormal presence of fibrous components (collagen, reactive glia) and likely represent two consecutive temporal characteristics of the same phenomenon.[13,17] We identified two subtypes of iERM in high-resolution adaptive optics images according to the distribution pattern of microfolds over the foveal area: a radial-type, showing radial folds covering the fovea, and a grid-type, showing numerous folds intersecting each other at random angles over the fovea. In this study, there were no specific differences in SD-OCT retinal cross sections between the two subtypes of iERM over the fovea. Larger-population study may clarify whether the different distribution of microfolds may lead to different directional forces on the retina and thus different disorganization of the inner and outer retinal layers.[1,18]
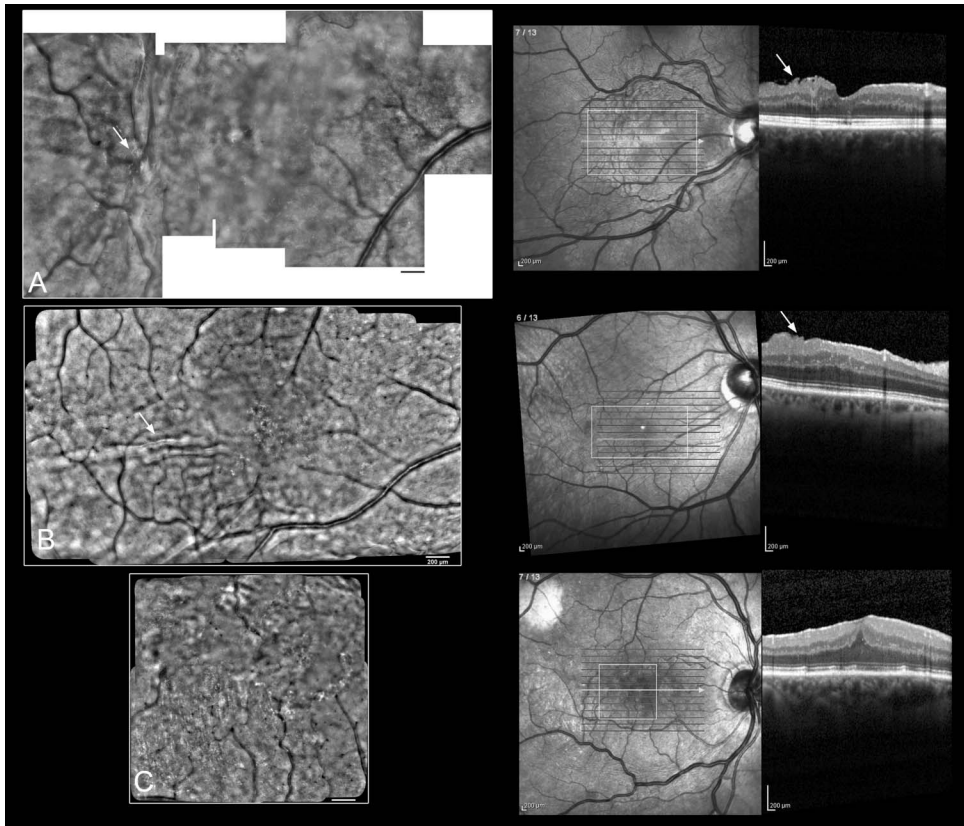
Fig. 4. En face adaptive optics and cross-sectional SD-OCT imaging of the retina in Cases 2 and 3, which had no ILM removal, and Case 4 (radial-type iERM, ILM removed) at 12 months after surgery. Scale bars represent 200 μm. **A** and **B.** In Cases 2 and 3, the macrofolds were still resolvable at the vitreomacular interface at the end of follow-up. These folds correlated with distorted profile of the inner retina (arrows). Dot or ring-shaped hyperreflective features were visible over the fovea. **C.** In Case 4, the hyperreflective microstructures run along the Müller septa, parallel to the nerve fiber bundles.

Morphologic study of iERM based on complementary information provided by high-resolution en face and cross-sectional images of the retinal tissue will enhance the clinical utility of imaging-based technology to screen and monitor disease progression and efficacy of surgery.

After surgery, the number of macrofolds greatly decreased in all cases. All the macrofolds disappeared at 1 month postoperatively, except for Cases 2 and 3, indicating that they were associated with the fibrous component of iERM responsible for retinal wrinkling and folding. Internal limiting membrane removal was not done in Cases 2 and 3, which however showed the thickest mean CRT preoperatively. At the end of follow-up, the mean CRT decreased by 324 μm (−51%) and 267 μm (−38%), respectively; these changes were significantly greater than in cases that had ILM removal.

It is still object of controversies whether the presence of ILM may contribute to increase the recurrence rate of operation after iERM removal or not.[19] Several laboratory studies[20–27] have identified different contractile cellular (glial cells, fibroblastlike, hyalocytes) and extracellular (collagen, actin, fibronectin) elements of the ILM that may effectively contribute to recurrence. However, it cannot be excluded that remnants of primary epiretinal membrane may contribute to fibrocellular proliferation at the retinal surface.[28,29] Overall, the formation and recurrence of epiretinal membrane might be considered as an aberrant wound-healing process with multifactorial origin. Despite the increasing interest of this issue across retinal specialists,[19] this is the first study aiming at evaluating the microstructural changes of retinal architecture and vitreomacular interface in eyes that had ILM removal or not. Prospective studies with large populations are needed to clarify whether the persistence of ILM represents the real cause of the recurrent disorganization of the retina after surgery for iERM.

The ILM removal, with or without the use of vital dye, might damage the inner retinal microstructures. The procedure includes removal of the basement membrane, Müller cells' processes, and sometimes neurites and small vessels,[1,27] which may lead to microscopic or macroscopic damage to the inner retina.[10,30] Previous studies have shown "dissociated optic nerve fiber layer" or "concentric macular dark spots" in eyes that had ILM removal[30–33]; in this study, we did not find dark dots along the course of retinal nerve fibers in the area of ILM peeling in any case. However, these abnormal features of the vitreomacular interface have been shown to occur mainly after macular hole surgery

Table 2. One-millimeter CRT, Inner Retinal Thickness, and Outer Retinal Thickness Values During Follow-up

Study Case	1-mm Maximum CRT, μm				1-mm Minimum CRT, μm				1-mm CRT, μm			
	1 Month	3 Months	6 Months	12 Months	1 Month	3 Months	6 Months	12 Months	1 Month	3 Months	6 Months	12 Months
1	470	456	436	425	424	398	369	363	451	416	403	391
2	428	414	401	379	273	264	252	241	342	334	322	310
3	545	506	477	453	473	413	404	400	512	462	442	428
4	488	468	465	468	406	396	387	384	446	433	426	425
5	470	420	407	403	424	355	350	345	413	394	386	386
6	433	424	419	Unavailable	352	340	324	Unavailable	394	379	375	Unavailable
Mean	472	448	434	426	392	361	348	347	426	405	392	388
SD	42	36	31	36	70	55	55	63	58	45	42	48

Study Case	1-mm Central Inner Retinal Thickness, μm				1-mm Central Outer Retinal Thickness, μm			
	1 Month	3 Months	6 Months	12 Months	1 Month	3 Months	6 Months	12 Months
1	237	210	200	186	214	206	203	205
2	171	159	144	129	171	175	178	181
3	277	221	211	201	235	241	231	227
4	225	219	212	211	221	214	214	214
5	214	197	183	185	199	197	203	201
6	192	171	163	Unavailable	202	208	212	Unavailable
Mean	219	196	185	182	207	207	207	206
SD	37	37	28	32	22	22	17	17

when the ILM has been peeled.[30–33] In Case 5, several microcysts (13–46 μm diameter) were visualized by adaptive optics imaging over the vitreomacular interface at 6 months postoperatively. These findings correlated with dimples of the retinal nerve fiber layer and the presence of abnormal fluid in the corresponding inner retinal layers in SD-OCT images. This result suggests that alteration of the retinal nerve fiber layer in cross-sectional SD-OCT images is always associated with (micro- or macro-) damage to inner retinal microstructures. Nevertheless, 10° central sensitivity improved in all cases after surgery, except for Cases 6 and 3 that showed a slight decrease at 6 months and 12 months, respectively, because of cataract formation. Overall, the results of retinal function recovery after surgery for iERM were consistent with previous work.[18]

The hyperreflective structures have been already described in eyes with iERM[13] but the significance of these structures was unclear. In this work, we provided the novel information that these hyperreflective structures change their shape and morphology after surgery. Preoperatively, these microstructures were clustered in dots or short irregular lines over the vitreomacular interface and were not associated with any pathologic findings of the inner retina in SD-OCT images. After surgery, the hyperreflective features were greatly reduced in all cases, except for Cases 1, 4 and 6, all of which had ILM removal. In these cases, we recorded the lowest mean CRT thinning over time. All the hyperreflective microstructures were clearly distributed along the Müller septa and were undetectable by SLO or SD-OCT imaging. Preoperatively, the hyperreflective features might correspond to microexudates residing within the Müller septa or degenerated neurites and/or hyalinized retinal vessels of the inner retina caused by epiretinal membrane traction or to new fibrous tissue residing under the epiretinal membrane.[1] Postoperatively, these microstructures may be directly related to the traumatic removal of neurites and Müller cell processes induced by surgical manipulation of the vitreomacular interface mainly after ILM removal.

Scoles et al[34] have identified seven categories of hyperreflective microstructures of either the inner retina or the epiretinal interface in adaptive optics–SLO images acquired from eyes suffering from different retinal or neurologic diseases. Because these structures were not disease-specific, the authors hypothesized that they might correspond to common mechanisms of degeneration or repair in pathologic states. We found high similarities between their epiretinal granular category and the preoperative morphology of hyperreflective microstructures in eyes with iERM. After

surgery, there were no similarities between any of their seven categories and the hyperreflective features running along the Müller septa. It remains to be investigated whether these microstructures are disease-specific or represent common features to other surgical treatments.

In conclusion, adaptive optics imaging gives new insight into the changes of vitreomacular interface after iERM surgery. The combined monitoring of the vitreomacular interface and retinal structures can be valuable to understand the relationship between their pathologic changes and surgical outcome, leading to better management of patients. In addition, it may provide novel biomarkers of surgical outcome and become of interest to better clarify the pathophysiology of iERM.

Key words: adaptive optics, idiopathic epiretinal membrane, optical coherence tomography, pars plana vitrectomy.

References

1. Bu SC, Kuijer R, Li XR, et al. Idiopathic epiretinal membrane. Retina 2014;34:2317–2335.
2. Sandali O, El Sanharawi M, Basli E, et al. Epiretinal membrane recurrence: incidence, characteristics, evolution, and preventive and risk factors. Retina 2013;33:2032–2038.
3. Park DW, Dugel PU, Garda J, et al. Macular pucker removal with and without internal limiting membrane peeling: pilot study. Ophthalmology 2003;110:62–64.
4. Treumer F, Wacker N, Junge O, et al. Foveal structure and thickness of retinal layers long-term after surgical peeling of idiopathic epiretinal membrane. Invest Ophthalmol Vis Sci 2011;52:744–750.
5. Mirza RG, Johnson MW, Jampol LM. Optical coherence tomography use in evaluation of the vitreoretinal interface: a review. Surv Ophthalmol 2007;52:397–421.
6. Hwang JU, Sohn J, Moon BG, et al. Assessment of macular function for idiopathic epiretinal membranes classified by spectral-domain optical coherence tomography. Invest Ophthalmol Vis Sci 2012;53:3562–3569.
7. Legarreta JE, Gregori G, Knighton RW, et al. Three-dimensional spectral-domain optical coherence tomography images of the retina in the presence of epiretinal membranes. Am J Ophthalmol 2008;145:1023–1030.
8. Koo HC, Rhim WI, Lee EK. Morphologic and functional association of retinal layers beneath the epiretinal membrane with spectral-domain optical coherence tomography in eyes without photoreceptor abnormality. Graefes Arch Clin Exp Ophthalmol 2012;250:491–498.
9. Kang KT, Kim KS, Kim YC. Surgical results of idiopathic and secondary epiretinal membrane. Int Ophthalmol 2014;34:1227–1232.
10. Rispoli M, Le Rouic JF, Lesnoni G, et al. Retinal surface en face optical coherence tomography: a new imaging approach in epiretinal membrane surgery. Retina 2012;32:2070–2076.
11. Ooto S, Hangai M, Takayama K, et al. High-resolution imaging of the photoreceptor layer in epiretinal membrane using adaptive optics scanning laser ophthalmoscopy. Ophthalmology 2011;118:873–881.

12. Park SS, Choi SS, Zawadzki RJ, Werner JS. Fine retinal striae associated with epiretinal membrane visualized using adaptive optics. Retin Cases Brief Rep 2009;3:233–236.

13. Lombardo M, Scarinci F, Ripandelli G, et al. Adaptive optics imaging of idiopathic epiretinal membranes. Ophthalmology 2013;120:1508–1509.e1.

14. Lombardo M, Serrao S, Devaney N, et al. Adaptive optics technology for high-resolution retinal imaging. Sensors 2013; 13:334–366.

15. Drasdo N, Fowler CW. Non-linear projection of the retinal image in a wide-angle schematic eye. Br J Ophthalmol 1974; 58:709–714.

16. Lombardo M, Serrao S, Ducoli P, Lombardo G. Variations in the image optical quality of the eye and the sampling limit of resolution of the cone mosaic with axial length in young adults. J Cataract Refract Surg 2012;38:1147–1155.

17. Fraser-Bell S, Guzowski M, Rochtchina E, et al. Five-year cumulative incidence and progression of epiretinal membranes: the Blue Mountains Eye Study. Ophthalmology 2003;110: 34–40.

18. Mayer WJ, Vogel M, Neubauer A, et al. Pars plana vitrectomy and internal limiting membrane peeling in epimacular membranes: correlation of function and morphology across the macula. Ophthalmologica 2013;230:9–17.

19. Chang S. Controversies regarding internal limiting membrane peeling in idiopathic epiretinal membrane and macular hole. Retina 2012;32:S200–S204.

20. Gandorfer A, Rohleder M, Kampik A. Epiretinal pathology of vitreomacular traction syndrome. Br J Ophthalmol 2002;86: 902–909.

21. Gandorfer A, Haritoglou C, Scheler R, et al. Residual cellular proliferation on the internal limiting membrane in macular pucker surgery. Retina 2012;32:477–485.

22. Snead DR, James S, Snead MP. Pathological changes in the vitreoretinal junction 1: epiretinal membrane formation. Eye (Lond) 2008;22:1310–1317.

23. Kohno RI, Hata Y, Kawahara S, et al. Possible contribution of hyalocytes to idiopathic epiretinal membrane formation and its contraction. Br J Ophthalmol 2009;93:1020–1026.

24. Oberstein SY, Byun J, Herrera D, et al. Cell proliferation in human epiretinal membranes: characterization of cell types and correlation with disease condition and duration. Mol Vis 2011; 17:1794–1805.

25. Bringmann A, Wiedemann P. Involvement of Müller glial cells in epiretinal membrane formation. Graefes Arch Clin Exp Ophthalmol 2009;247:865–883.

26. Tari SR, Vidne-Hay O, Greenstein VC, et al. Functional and structural measurements for the asessmenst of internal limiting membrane peeling in idiopathic macular pucker. Retina 2007; 27:567–572.

27. Kostantinidis L, Uffer S, Bovey EH. Ultrastructural changes of the internal limiting membrane removed during indocyanine green assisted peeling versus conventional surgery for idiopathic macular epiretinal membrane. Retina 2009;29:380–386.

28. Kampik A, Pathology of epiretinal membrane, idiopathic macular hole, and vitreomacular traction syndrome. Retina 2012; 32:S194–S199.

29. Seidel G, Weger M, Stadlmüller L, et al. Association of preoperative optical coherence tomography markers with residual inner limiting membrane in epiretinal membrane peeling. PLoS One 2013;8:e66217.

30. Tadayoni R, Paques M, Massin P, et al. Dissociated optic nerve fiber layer appearance of the fundus after idiopathic epiretinal membrane removal. Ophthalmology 2001;108:2279–2283.

31. Mitamura Y, Ohtsuka K. Relationship of dissociated optic nerve fiber layer appearance to internal limiting membrane peeling. Ophthalmology 2005;112:1766–1770.

32. Alkabes M, Salinas C, Vitale L, et al. En face optical coherence tomography of inner retinal defects after internal limiting membrane peeling for idiopathic macular hole. Invest Ophthalmol Vis Sci 2011;52:8349–8355.

33. Kusuhara S, Matsumiya W, Imai H, et al. Evaluating dissociated optic nerve fiber layer appearance using en face layer imaging produced by optical coherence tomography. Ophthalmologica 2014;232:170–178.

34. Scoles D, Higgins BP, Cooper RF, et al. Microscopic inner retinal hyper-reflective phenotypes in retinal and neurologic disease. Invest Ophthalmol Vis Sci 2014;55:4015–4029.